221 803

UCRL-JC-113393
PREPRINT

Velocity and Attenuation Structure of the Geysers Geothermal Field, California

J.J. Zucca
L.J. Hutchings
P.W. Kasameyer

This paper was prepared for submittal to
Journal of Geophysical Research

February 23, 1993

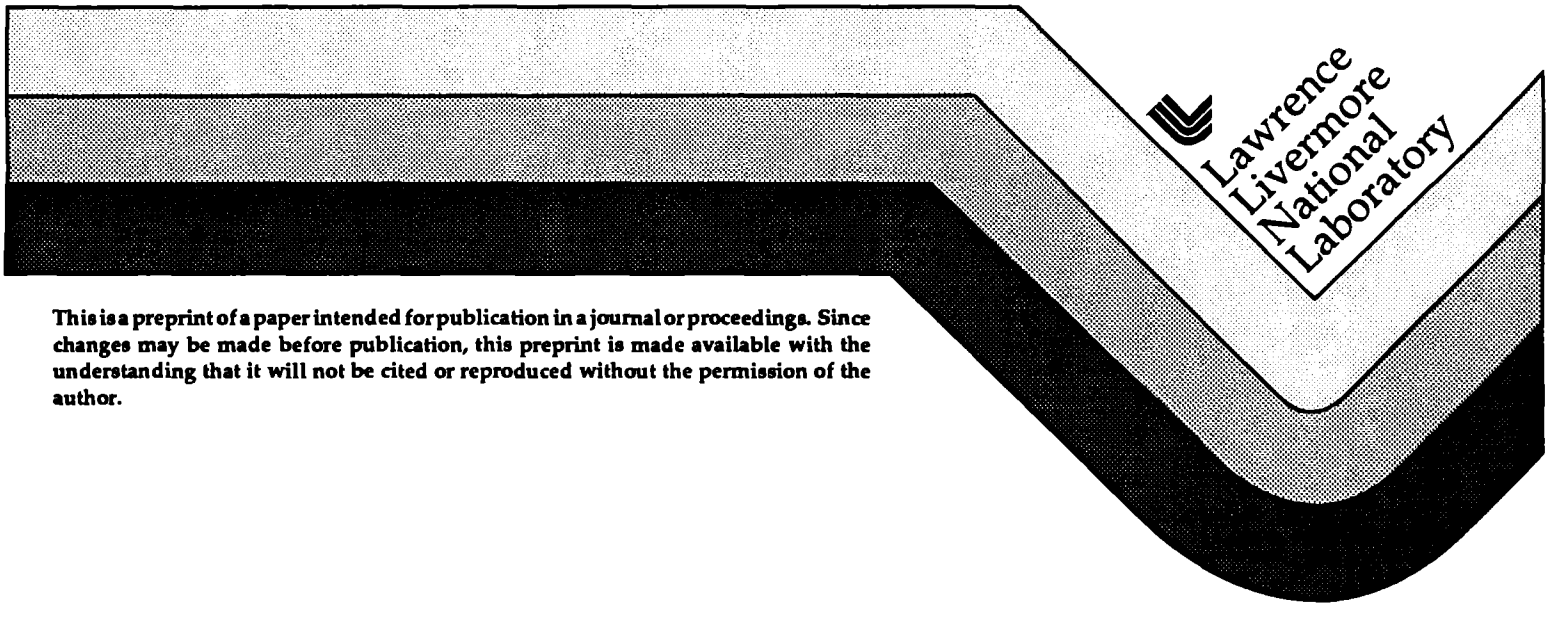

Velocity and Attenuation Structure of the Geysers Geothermal Field, California

J. J. Zucca, L. J.Hutchings, and P. W. Kasameyer
Lawrence Livermore National Laboratory
P.O. Box 808, Livermore, CA 94551

Last edit: Feb. 23, 1993

To be submitted to the
Journal of Geophysical Research

Abstract

The Geysers geothermal field is located in northern California and is one of the world's largest producers of electricity from geothermal energy. The resource consists of primarily dry steam which is produced from a low, porosity fractured graywacke. Over the last several years steam pressure at the Geysers has been dropping. Concern over decline of the resource has prompted research to understand its fundamental nature. A key issue is the distribution of fluid in the matrix of the reservoir rock. In this paper we interpret seismic compressional-wave velocity and attenuation data at the Geysers in terms of the geologic structure and fluid saturation in the reservoir. Our data consist of approximately 300 earthquakes that are of magnitude 1.2 and are distributed in depth between sea level and 2.5 km. Using compressional-wave arrival times, we invert for earthquake location, origin time, and velocity along a three-dimensional grid. Using the initial pulse width of the compressional-wave, we invert for the initial pulse width associated with the source, and the one-dimensional Q structure. We find that the velocity structure correlates with known mapped geologic units, including a velocity high that is correlated with a felsite body at depth that is known from drilling. The dry steam reservoir, which is also known from drilling, is mostly correlated with low velocity. The Q increases with depth to the top of the dry steam reservoir and decreases with depth within the reservoir. The decrease of Q with depth probably indicates that the saturation of the matrix of the reservoir rock increases with depth.

Introduction

The Geysers geothermal field accounts for approximately 9% of PG&E's power production for the state of California. It has become an area of focused study since it was make known that steam pressure has been declining at an increased rate since 1981 (Barker *et al.*, 1989). A better understanding of the physical processes at work within the field could help moderate that trend. Specifically, a means to remotely determine the boundaries of the

reservoir, the distribution of steam and two-phase fluid within the field, and the changes in that distribution as a result of production and injection is needed. To this end, we are investigating a means to compute images of the seismic velocity and attenuation structure of the region and to jointly interpret these data for the location and *in situ* phase state of water in the reservoir.

In this paper, we compute a three-dimensional velocity structure of the Geysers. We also describe and use a new procedure for the computation of the P-wave seismic quality factor, Q, using pulse widths. We do not invert simultaneously for velocity and Q. Rather, we assume that there is independent information in the Q structure that can complement the interpretation of the velocity structure. Our procedure is to first use arrival times for a simultaneous nonlinear inversion for velocity structure and hypocentral location. The velocity structure and ray paths are then held fixed and pulse widths of the first-arriving P-waves are inverted for Q structure and the source contribution to the pulse-width. We used a modified Thurber (1983) algorithm (Eberhart-Phillips, 1988, personal communication) for inversion of P-wave travel times and modified the Thurber algorithm further to invert for Q structure.

In previous studies, we used spectral ratios to compute relative attenuation differences that were jointly interpreted with velocity variations computed from relative residuals (Evans and Zucca, 1988: and Zucca and Evans, 1992). As discussed more fully below, in this case we use pulse widths because of their direct analog to the local earthquake velocity structure inversion problem. Furthermore, the ray assumption is more valid. Spectral estimates are based on several cycles of the P-waves, so that the travel path is not well known. Whereas, pulse widths use only the very first part of the first arrival, the ray assumption is more valid.

As in the earlier papers (Evans and Zucca, 1988: and Zucca and Evans, 1992), we use the velocity and Q data to interpret the structure of the target geothermal region, in this case the Geysers, in terms of the existence of pore water and its phase state. We base our

interpretation primarily on the laboratory data of Ito *et al.* (1979) who carried out velocity and attenuation measurements on Berea sandstone samples at elevated temperatures and varying degrees of saturation to approximate reservoir conditions. Their measurements show that P-velocity increases with saturation but that Q decreases. In addition, Q falls dramatically when the rocks are partially saturated. These laboratory results were for frequencies near 10,000 Hz, raising the question of their applicability to field measurements at lower frequencies. However, results from Evans and Zucca (1988) and Zucca and Evans (1992) show that P-wave attenuation and seismic velocity structure contain complimentary information at Medicine Lake and Newberry volcanoes, and may be used to predict the location of geothermal drilling targets. They found that regions with low Q and normal-to-high P-wave velocity are suggestive of boiling water, in areas independently identified as good geothermal prospects by other means.

Previous Geological and Geophysical Work at the Geysers

The stratigraphy and geology of the Geysers have been recently summarized by McNitt *et al.* (1989) who attempted to correlate the earlier mapping efforts by Bailey (1946), McNitt (1968), and McLaughlin (1981). For our target volume, we summarize the results of McLaughlin (1981) in figure 1. The surface geology of the target volume consists mostly of Franciscan melange rocks with young volcanic rocks covering the east corner. An ultramafic stringer extends northwest-southeast across the volume. The structural grain dips to the north. The Big Sulfur Creek fault zone is one of many regional faults.

McNitt (1989) also compiled the results of several hundred lithologic logs for the Geysers region to develop a model of the stratigraphy at depth. They conclude that the steam reservoir is contained in a highly indurated and fractured graywacke which is capped with a more ductile, unfractured argillaceous graywacke. The graywacke sequence has been intruded at its base by silicic magmas to form a felsite batholith whose axis trends northwest and is roughly coincident with the steam field (Thompson, 1989). The depth to the top of the steam reservoir and to the top of the felsite intrusive body have recently been made public by

a consortium of Geysers operators (Industry Consortium, 1989). These contour maps have been reproduced for our target volume in figure 1.

Extensive geophysical studies have been carried out at the Geysers. We summarize here the most recent and relevant results to our study area. A three-dimensional block inversion for P-wave structure for the Geysers and its surrounding area was done by Eberhart-Phillips (1986), using the Thurber (1983) method. She used P-wave arrivals from the USGS network to record local earthquakes and refraction shots. The resolution achieved was to 2 to 3 km. O'Connell and Johnson (1991) performed a progressive inversion for hypocenters and P-wave and S-wave velocity structure of the Geysers in much of the same area as the current study. Their resolution was 1-km. In this study, we increase resolution to approximately 0.6 km (*i.e.* 2000 ft).

The seismicity of the area has also been studied extensively to investigate induced seismicity due to steam production. Examples of this work are Stark (1989) and Eberhart-Phillips and Oppenheimer (1984). Eberhart-Phillips and Oppenheimer found that seismicity is affected by steam production and fluid injection. Stark found a correlation between seismicity and injection of fluids. Majer and McEvilly (1979) have conducted seismicity and seismic refraction studies at the Geysers. They note that the upper part of the reservoir is characterized by high velocities and low attenuation. Majer and McEvilly did not attempt a three-dimensional interpretation of their data.

Pulse Width as a Measure of Q

In the idealized situation of linear propagation of a signal through a medium with intrinsic Q, the frequency content of the signal is modified by the attenuation operator:

$$A(\omega) = A_0(\omega) e^{\frac{-\omega R}{VQ}} \qquad (1)$$

where $A(\omega)$ is the Fourier amplitude, R is ray travel distance, V is seismic velocity, and Q is the attenuation quality quotient, assumed to be independent of frequency. In the time

domain it is shown by Gladwin and Stacey (1974) and Kjartansson (1979) that the attenuation operator acts to broaden the pulse width by a factor proportional to R / VQ.

Our data suggest that pulse broadening is a reasonable model for estimating Q at the Geysers, because we observe that pulse widths systematically broaden along the travel path. Figure 2 shows pulse shapes from a single earthquake recorded at several stations at the Geysers. The pulse widths vary by up to a factor of 3 between stations, with more distant stations having broader pulse widths. However, inverting pulse widths for Q structure involves several issues that have not been fully resolved in the literature. Issues that need to be addressed are: the relative contribution of scattering and intrinsic Q to pulse broadening; the contribution of the source to the observed pulse widths; the f_{max} effect on pulse width; and determining the most appropriate mathematical model for pulse broadening as a function of Q. These issues are discussed in the rest of this section.

Intrinsic and scattering Q (Richards and Menke, 1983) affect the seismic signals by different mechanisms. As described above, intrinsic Q removes high frequency energy from the entire wavetrain, with the arrivals that travel along the longest ray paths having the greatest loss of high frequencies. On the other hand, Richards and Menke also show that scattering delays the arrival of the high frequency energy which tends to broadens the initial pulse. They propose a test to see if the signal is dominated by intrinsic or scattering Q. If scattering is affecting pulse width, then the corner frequency of the early parts of the wavetrain would be lower than in the later parts. If intrinsic Q were dominant, no increase in corner frequency would be observed later in the wavetrain. We examined several events for this effect by computing corner frequencies for two adjacent 0.5 s time windows following the first arrival. Care was taken not to include the S-wave arrival. We found no systematic increase in corner frequency in the later time window. We conclude that scattering attenuation is not the dominant attenuation mechanism.

The finite duration of the seismic source can contribute to the observed pulse width. The contribution of the source to pulse width is evident from figure 3 where pulse width is plotted

as a function of distance from the hypocenter for our data. It is apparent from the figure that pulse width generally increases with distance, that the data exhibit a large noise component, and that there is a finite pulse width at zero travel time. There may also be some contribution to pulse width due to directivity, but we deliberately chose earthquakes that are small enough to minimize this effect. Furthermore, since focal mechanism affects amplitude and not spectral content, we expect no pulse width variation from this effect.

A mathematical model for realistic pulse broadening in an inhomogeneous medium has been suggested by Gladwin and Stacey (1974) and Stacey *et al.*, (1975). They showed experimentally that a pulse propagating in an elastic medium has a pulse width that follows the relation:

$$\tau = \tau_0 + C \int_{ray} \frac{ds}{V_0(r)Q(r)} \qquad (2)$$

where C a constant (Stacey *et al.*, uses 0.5), ds is distance along ray path, and τ_0 is the source contribution to the original pulse width (Stacey *et al.*, used zero for this term), and $V_0(r)$ is the velocity structure that varies as position r. τ is the time from the onset of the initial arrival to the initial peak on displacement records, or the first zero crossing on velocity records. This is the relation used in this study. It is supported by the linear trend of pulse broadening observed in figure 3. The source term, τ_0, is a significant contributor to pulse width as shown above and discussed statistically below.

It has been suggested that attenuation inversion is not possible in areas with very low Q values near the surface, because a very low intrinsic Q value over a short distance can cause pulse-broadening large enough to mask all previous effects on pulse widths. This is referred to as the f_{max} effect (Hanks ,1982; Frankel, 1982; Hutchings, 1990). Majer (1979) apparently observed this effect at the Geysers. He found that earthquakes below a magnitude of approximately 2.0 in the Geysers had corner frequencies that were independent of seismic moment, indicating that the initial spectral shape (or pulse width) from the source was masked. Figure 4 shows pulse widths from our study observed at a single station from

several events of similar magnitude (1.2-1.4) distributed across the study area. The variation in pulse widths is up to a factor of 3, which is inconsistent with a low Q surface layer. It is also apparent that there is not a systematic broadening of the pulse from more distant events. This observation is in apparent conflict with the pulse broadening with distance shown in figure 3, except that in the case of figure 4 the observed variation in pulse width is partially due to the initial pulse width from the source. These observations contradict those of Majer (1979) and may be a result of differences in recording location.

Inversion Approach

We used the Thurber inversion method (Thurber, 1983) as modified by Eberhart-Phillips (personal communication, 1989) to compute a three-dimensional model of velocity and a one-dimensional model of Q. As normally implemented, the Thurber method uses locally-occurring earthquakes or explosions as sources and P- and S-wave arrival times as input data. We use only P-waves from local earthquakes. The inversion solves for both earthquake location and velocity structure by minimizing the residuals of travel times computed as:

$$t = t_0 + \int_{ray} \frac{ds}{V(r)} \tag{3}$$

where t_0 is origin time and $V(r)$ is the velocity structure.

Recognizing that the relationship between QV and t is the same as the relationship between V and t, we inverted pulse widths for Q structure by modifying the Thurber routine to accept pulse width data as input. The travel time inversion was carried out first to determine velocity which was then passed on to the pulse width inversion as $V_0(r)$ in equation 2. The major advantage of using the Thurber program for inversion of pulse widths is its direct analog with the travel time inversion.

Data

The UNOCAL-NEC-Thermal (U-N-T) partnership has monitored portions of the Geysers geothermal field since 1985 (Stark, 1989). Waveforms from events are digitally recorded at

100 samples per second and archived by U-N-T in Santa Rosa, California. The network records 15,000 to 20,000 events per year that have an mean local magnitude of approximately 0.7. Depths for the events are fairly evenly distributed to about 2.5 km (below sea level). Although events do cluster in certain regions, there are sufficient events to provide sources in most areas for our inversion. Events used in this study occurred during the time period of May 1988 to December 1989. Figure 5 shows the distribution of stations and events. Table 1 lists all stations available for this study.

U-N-T provided us with waveforms and hand-picked first arrivals (Debbie Turner, personal communication, 1990). Because of the abundance of data, we selected the best events to further process and obtain P-arrival times and pulse widths. We used only arrivals with at least 10:1 signal-to-noise ratio of the first pulse observed at 8 or more stations. The time between the first arrival and the first zero crossing was used to measure the pulse widths. We examined each pulse by eye for evidence of multipathing. We accepted only those pulses that were smooth from the initial arrival to the first zero crossing. The first arrival pick was also examined by eye to see if further adjustment was necessary. The estimated error in the arrival time reading is less than +0.01 s (one sided error). The measurement error in the first zero crossing is small compared to the error in the first arrival pick.

The picking error is small compared to travel times, and their contribution to errors in event locations and determination of velocity structure is small. However, the picking error is a substantial percentage of the pulse widths, which vary from 0.025 to 0.052 s. The noisy data limited the number of Q model parameters for which we could invert.

Inversion Initial Conditions

The Thurber inversion code uses a node system to specify inversion parameters. Velocity or Q values are specified at the node intersections and are bi-linearly interpolated to compute the parameter between the node points. Choice of node spacing is important to the final result. As a general rule, the spacing should be as small as practical. Too coarse a grid

can result in poor fidelity, spatial aliasing, and entirely missing some parameter variations (Toomey and Foulger, 1989; Ellsworth, 1977; Evans and Achauer, 1992). At a minimum, the node spacing should not be less than the Fresnel zone (Nolet, 1987), which is the maximum spatial deviation between two ray paths that allows them to constructively interfere (*i.e.* a 1/4 wave length). The maximum Fresnel spacing for the current study is approximately 0.5 km. Furthermore, the node spacing should not be so small that there are more parameters than observations.

A further consideration is the structure of the resolution matrix. Evans and Achauer (1992) consider the effect of the progressive decrease of node spacing on the resolution matrix and the inversion results. They point out that in inversion problems where the rays are sub vertical, the individual rows of the resolution matrix tend to have positive side lobes above and below the parameter in question and negative side lobes horizontally around the parameter in question. Too fine a parameterization can cause artifacts to develop in the spaces between parameters when the node spacing is decreased below the minimum horizontal ray spacing. They suggest an offset and average procedure to horizontally smooth the results. We adapted this procedure for Thurber style inversions by averaging the results from the base grid system and three variants, which are obtained from the base system by offsetting it along the x- and y-axes one-half grid spacing. Our base grid system is shown in figure 1. It has a spacing of 0.6 km (*i.e.* 2000 ft) in all three directions. The datum is sea level.

In general, the results of non linear inversion depend on the starting model. Foulger and Toomey (1989) investigated the dependence of their results on the starting model and concluded that although their results did indeed depend on the starting model, the differences in the results were not significantly different given the accuracy of their arrival time data. Fortunately, at the Geysers there is ample previous work to establish a realistic velocity model which should mitigate the effects of starting model dependence if there is any.

To locate micro-earthquakes at the Geysers, U-N-T uses a one-dimensional model which is based on the results of Eberhart-Phillips (1986; M. Stark, personal communication, 1990, table 2). However, more local detailed information is available. Majer *et al.*(1988) conducted vertical seismic profiling to a depth of 5100 ft (1555 m) in the northern extreme of our study area near station s09. O'Connell and Johnson (1991) used these results to derive a one-dimensional model in the upper 4000 ft (1200 m), having velocities approximately 3.0 km/s compared to the U-N-T model which is approximately 4.0 km/s at these depths. For our study region, we find that the U-N-T starting model results in the lowest overall residuals. However, widely varying near-surface geology may make the U-N-T model inappropriate for some local areas in the near surface structure. To accommodate these variations, station corrections were included in the inversion.

The inversion for Q also requires a starting model which we chose as the average Q for the target volume. This was obtained by finding the slope of a straight line fit to plots of pulse width as a function of travel time. The slope is related to Q through equation 1. The average value of Q was found to be 65 which agrees quite well with the average Q of 60 used by Majer and McEvilly (1979) in their study.

Inversion Results

The three-dimensional inversion for velocity resulted in a 75% weighted variance reduction over the one-dimensional starting model. Three different weighting criteria were used. Arrivals were weighted according to quality determined during hand picking, travel paths longer than 15 km were down weighted, and residuals greater than 0.1 s were down weighted. The final weighted RMS was 0.012 s which is slightly larger than the picking error of 0.01 s. The final damping parameter was chosen subjectively based on tradeoffs between data variance, solution length, diagonal resolution value, and standard error size. The damping was initially picked so that small changes in data variance would not result in large changes in solution length. We then fine-tuned the selection of the damping parameter so that 'reasonable' values of the resolution matrix diagonals and standard errors were

achieved. The distribution of the resolution values for the layers being interpreted is shown in figure 6.

The velocity inversion results are shown in figure 7. The results are displayed as horizontal slices through the three-dimensional velocity volume. Although the model extends to a depth of almost 4 km, we present only the four layers that represent the surface to 1.5 km depth. The resolution drops off dramatically below this layer and it has lesser relevance to the geothermal reservoir. The color scale is the same for all four cross-sections. In general, the velocity increases with depth. The central portion of the model tends to have the highest relative velocities down to at least the 0.9 km depth level. At the deepest level shown at 1.5 km depth, the lower (*i.e.* south) part the image has the highest overall velocities.

The velocity inversion fixed the source locations and ray paths therefore, these parameters do not need to be determined in the inversion for attenuation. The parameters we did invert for are the initial pulse width and the Q structure. The initial pulse widths range from 0.018 to 0.048 s. Subtracting the initial pulse widths from the pulse widths shown in figure 3 exacerbates the noise problem and makes the data more difficult to invert. To test model significance we tried many levels of the inversion starting with a simple one-dimensional model with Q varying only with depth to models with only a few nodes, to models with as many nodes as the velocity model. We were only able to achieve significant data variance reduction with the one-dimensional model. The 1D model had a starting data variance of 0.000309 s and a final data variance of 0.000073 s after calculation of the source term and Q variations. This is a net variance reduction of 76%, however most of this is due to solving for τ_0, the source contribution to the pulse width. Only about 15% of the variance reduction is due to the structure. The Q results are shown adjacent to the velocity results in figure 7.

Interpretation

Our uppermost layer (layer 1 at –0.3 km depth) is completely above the reservoir and should be influenced mostly by the surface geology. McLaughlin (1981) has published a

geologic map of the region which we have generalized for our target volume in figure 7. Our observed high-velocity body in the center of this layer correlates at its south end with the ultramafic stringer and continues to the northeast, which implies a dip to the north of the body which agrees with McLaughlin's map and cross section. The apparent pinchout of the high-velocity body to the southeast is probably the result of the loss of resolution in that corner of the model (see figure 6).

The next layer is at 0.3 km depth. It intersects the reservoir at three cupolas, one each in the north, west, and south of the layer (figure 7). The northern cupola is clearly associated with a low-velocity zone. The western one is only partially associated with low velocity and the southern one is not associated with any change in velocity. The next layer down at 0.9 km depth intersects more directly with the reservoir and the part of the layer within the reservoir is clearly associated with low velocity.

The deepest layer is at 1.5 km depth and is completely within the reservoir. At this depth we have overlaid the depth to the felsite intrusion which is associated with a blotchy series of high velocity anomalies. Although the felsite and the indurated graywacke reservoir rocks should have roughly equivalent velocity, the felsite is likely to be less fractured and could exhibit slightly higher velocity. The weak velocity contrast could explain the blotchy nature of its signature in the velocity image.

The velocity appears to be well correlated with what is known about the structure of the area from geologic mapping and drilling. We now attempt to add the attenuation to the interpretation and to infer the state of pore fluids in the target volume. We base our inferences on the laboratory data of Ito *et al.* (1979) discussed in the introduction. There is little direct information on the state of pore fluids at the Geysers since any water present in the formation flashes to steam upon entering the borehole or feeder fracture. Estimates for the liquid saturation range from 30 to 50% (Dykstra, 1981) to well above 50% (Pruess and Narasimhan, 1982). Our layer 3 (figure 7) is mostly in the reservoir and tends to have a high Q relative to the next layer down which is completely within the reservoir. The high Q in

the upper part of the reservoir is consistent with the earlier results of Majer and McEvilly (1979) who also found relatively high Q in this region. The low Q in the lower part of the reservoir suggests that the saturation is in the 30 to 70% range while saturation at the top of the reservoir could go up or down and still agree with the lab results for Q alone obtained by Ito et al. (1979). A drop in saturation at the top of the reservoir below about 30% seems the most likely since the velocity is lower in the reservoir compared to the country rocks indicating a drop in saturation compared to the country rocks.

Above the reservoir in layers 1 and 2 the Q increases with depth. The low Q at the surface reflects the small overburden which tends to leave micro cracks open and lower the Q. As depth increases, the lithostatic pressure increases and tends to close cracks and the Q increases.

The initial pulse widths due to the source duration vary from 0.023 to 0.052 s. A Brune source model predicts source duration of 0.01 to 0.02 s for the magnitude 1.0 to 1.2 events used. The observed variation in source duration is somewhat larger than the theory predicts but is not unreasonable and may be due to variations in stress drop or magnitude, or due to scatter due to the noisy pulse width data. We did not find any systematic variation with source duration within the target volume.

Conclusions

We have calculated the velocity and attenuation structure of the Geysers region using local earthquakes. Our data for the inversion consisted of P-wave arrival times and pulse widths which we used to compute three-dimensional compressional wave velocity structure and one-dimensional compressional wave attenuation structure. Our velocity structure correlates well with the surface geology and published studies on the structure of the reservoir. The reservoir appears to exhibit low velocity with the surrounding country rock. The Q decreases with depth which we infer to indicate partial saturation (30 to 70%) at depth with drier conditions near the top of the reservoir.

Unfortunately, the Q inversion was limited to computing one-dimensional variations because of the very noisy nature of the pulse width data. We feel the noise is primarily due to the error in the arrival time determination being large relative to the pulse width. We are currently collaborating with Lawrence Berkeley Laboratory to collect to much higher time resolution data in the southeast Geysers. We expect these data will yield more accurate pulse widths and a three-dimensional model of the Q structure.

Acknowledgments

The authors would like to thank Debbie Wheeler of UNOCAL for her great effort in preparing the data for us to use. Mitch Stark, Jens Pederson, and Bill Cummins, also of UNOCAL, help form our ideas during the course of the work with extensive technical discussions. This work was performed at the Lawrence Livermore National Laboratory and was supported under the Geothermal Technology Division and the Assistant Secretary for Conservation and Renewable Energy of the U.S. Department of Energy under contract W-7405-ENG-48.

Figure Captions

Figure 1. Geologic setting of inversion target volume. a) Generalized surface geology (after McLaughlin, 1981). b) Depth to top of dry steam reservoir (after Industry Consortium, 1989). c) Depth to top of felsite intrusive body (after Industry Consortium, 1989). d) Map view of inversion grid. Spacing is ~ 0.3 km (2000 ft) in all three directions. Datum is sea level. Note that north is to the upper left. Inset a bottom right shows location of the Geysers in the state of California.

Figure 2. Pulse width variations for a single event recorded at several stations. The map in the lower right shows the location of the station and events with respect to the target volume. Note that north is up.

Figure 3. Pulse widths plotted as a function of distance from hypocenter to receiver.

Figure 4. Pulse width variations for a single station from several events. The map shows locations relative to the target volume. Note that north is up.

Figure 5. Location of seismograph stations and earthquakes used in this study.

Figure 6. Distribution of the diagonals of the resolution matrix. The data are displayed as horizontal slices through the target volume. Layer numbers correspond to those in figure 7.

Figure 7. Velocity variations from U-N-T starting model displayed as horizontal depth slices. Slice depth is given at the corner of the images in kilometers below sea level. Overlay contours are depth to the feature below sea level. Squares indicate the location of power plant units. Q values for each layer are given on the left.

References Cited

Bailey, E.H. (1946) Quicksilver deposits of the western Mayacamas district, Sonoma county, California, Cal. J. Mines and Geology, vol. 42, no. 3, pp. 192-230.

Barker, B.J., M.S. Gulati, M.A. Bryan, and K.L. Riedel (1989) Geysers Reservoir Performance, Geoth. Res. Council Trans. (abs.), vol 13, page 349.

Dykstra, H. (1981) Reservoir assessment of the Geysers field—Reservoir engineering, report, California Div. Oil and Gas, Sacramento, April.

Eberhart-Phillips, Donna (1986) Three-dimensional velocity structure in northern California Coast Ranges from inversion of local earthquake arrival times. Bull. Seis. Soc. Am., 76, 1025-1052.

Eberhart-Phillips, D. and D. H. Oppenheimer (1984) Induced seismicity in the Geysers geothermal area, California, J. Geophys. Res., 89, 1191-1207.

Ellsworth, W.L. (1977) Three-dimensional structure of the crust and upper mantle beneath the island of Hawaii, Ph.D Thesis, Mass. Inst. Tech., Cambridge, U.S.A.

Evans, J.R. and J.J Zucca (1988) Active High-Resolution Tomography of compressional-wave velocity and attenuation structure at Medicine Lake Volcano Northern California Cascade Range, J. Geophys. Res., 93, 15,016–15,036.

Evans, J.R. and U. Achauer (1993) Teleseismic tomography using the ACH method, theory and application to continental-scale studies, in 'Seismic Tomography, Theory and Practice', ed. H.M. Iyer and K. Hirahara, Chapman and Hall pub., 848 pages.

Frankel, Arthur (1982) The effects of attenuation and site response on the spectra of microearthquakes in the northeastern Caribbean, Bull. Seis. Soc. Am., 72, 1379-1402.

Gladwin, M. T., and F. D. Stacey (1974) Anelastic degradation of acoustic pluses in rock, Phys. Earth Planet. Interiors, 8,332-336.

Hanks, T. C. (1982) f_{max}, Bull. Seis. Soc. Am., 72, 1867-1879.

Hutchings, Lawrence (1990) Empirical Green's functions from small earthquakes: A waveform study of locally recorded aftershocks of the 1971 San Fernando earthquake. J. Geophys. Res. 95, 1187-1214.

Ito, H., J. DeVilbiss, and A. Nur (1979) Compressional and shear waves in saturated rock during water-steam transition. J. Geophys. Res. 84, 4731-4735.

Industry Consortium (1989), Geysers, 'Top of Reservoir Map' and 'Top of Felsite Map', both maps compiled through the cooperative efforts of UNOCAL, Freeport-McMoRan Geysers Geothermal, Northern California Power Association, GEO, Santa Fe Minerals Inc., and the Department of Water Resources of the state of California, presented at the Geothermal Resources Council Annual Meeting, 1 - 4 Oct., Santa Rosa, CA.

Kjartansson, Einar (1979) Constant Q-wave propagation and attenuation. J. Geophys. Res. 84, 4737-4748.

Majer, E. L. and T. V. McEvilly (1979) Seismological investigations of the geysers geothermal field. Geophysics 44, 246-269.

Majer, E. L., T. V. McEvilly, F. S. Eastwood, L. R. Myer (1988) Fracture detection using P-wave and S-wave vertical seismic profiling at the Geysers. Geophysics, 53, 76-84.

McLaughlin, R.J., (1981) Tectonic steeing of pre-tertiaty rocks and its relation to geothermal resources in the Geysers-Clear Lake area, in *U.S. Geol. Surv. Prof. Pap. no. 1141*, pp. 3-24.

McNitt, J.R.,(1968) Geology of the Kelseyville quadrangle, Map sheet 9, Cal. Div. Mines and Geology.

McNitt, J.R., R.C. Henneberger, J.B. Koenig, and A. Robertson-Tait, (1989) Stratigraphic and structural controls of the occurrence of steam at the Geyers, Geothermal Resources Council Transactions, vol 13, 461-465.

Nolet, G. (1987), Seismic wave propagation and seismic tomography, in "Seismic Tomography with applications in global seismology and exploration geophysics" G. Nolet (ed.), D. Reidel Pub. Co., 386pp.

O'Connell, Daniel, and Lane R. Johnson (1991), Progressive inversion for hypocenters and P wave and S wave velocity structure: application to the Geysers, California, Geothermal Field, J. Geophys. Res., 96, 6223-6236.

Pruess, K., and T.N. Narasimhan (1982) On fluid reserves and the production of superheated steam from fractured, vapor-diminated geothermal reservoirs, J. Geophys. Res., vol. 87, 9329-9339.

Richards, P.G., and W. Menke (1983) The apparent attenuation of a scattering meduim, Bull. Seis. Soc. Am., 73, 1005-1022.

Stacy, F. D., M. T. Gladwin, B. McKavanagh, A. T. Linde, and L. M. Hastic (1975) Anelastic damping of acoustic and seismic pulses. Geophysical Survey, 2, 133-157.

Stark, Mitchel A. (1989) Imaging injected water in the Geysers reservoir using microearthquake data. Unocal Geothermal Corp., Santa Rosa, Ca.

Thompson, R. C., and R. P. Gunderson (1989) The orientation of steam-bearing fractures at the Geysers Geothermal Field, Geothermal Res. Council, Transactions, 13, 487-490.

Thurber, C. H. (1983) Earthquake locations and three-dimensional crustal structure in the Coyote Lake area, central California, J. Geophys. Res., 88 , 8226-8236.

Toomey and Foulger (1989) Tomographic inversion of local earthquake data fron the Hengill-Grensdalur central volcano complex, Iceland, J. Geophys. Res., 94, 17,497–17,510.

Zucca, J. J., and J. R. Evans (1991) Active high-resolution compressional-wave attenuation tomography at Newberry volcano, central California, J. Geophys. Res., 97, 11,047–11,055.

Table 1: Station locations used in this study. Starred station was not actually used but is shown for completeness to compare with U-N-T station names

Station ID	U-N-T ID	Lat (deg)	(min)	Lon (deg)	(min)	Elev (m)
s01	acr	38	50.20	122	45.51	800
s02	ang	38	48.17	122	45.04	1326
s03*	sblz	38	48.60	122	49.72	570
s04	sb2z	38	48.49	122	49.37	570
s05	sb3s	38	48.57	122	49.72	551
s06	sb4b	38	48.57	122	49.72	521
s07*	lckz	38	49.18	122	44.40	1172
s08*	bmtz	38	47.79	122	46.61	856
s09	cap	38	50.76	122	48.46	862
s10	inj	38	48.49	122	48.21	711
s11*	hvcz	38	50.63	122	46.76	790
s12	drk	38	47.31	122	48.15	747
s13*	glb	38	51.17	122	45.70	741
s14	buc	38	49.39	122	50.05	884
s15	sqk	38	49.41	122	48.53	683
s16*	gec	38	48.65	122	48.24	820
s17*	glb	38	51.17	122	45.70	741
s18*	uocz	38	98.65	122	46.67	1055
s19	dxrz	38	49.37	122	46.30	1006
s20	clv	38	50.32	122	47.35	991
s21	ul4	38	47.13	122	46.25	848
s22	fnfs	38	46.22	122	45.86	855
s23*	ul7	38	49.59	122	46.63	1047
s24*	ul7z	38	49.58	122	46.63	1047
s25*	beil	38	46.86	122	45.65	815
s26*	bei2	38	47.24	122	45.85	856
s27	bmr	38	47.66	122	46.90	777
s28	fum	38	47.59	122	47.20	646
s29*	cck	38	48.18	122	46.34	788
s30*	cck	38	48.17	122	46.34	788
s31*	toc	38	47.02	122	44,04	960
s32*	gdh	38	49.81	122	47.17	989
s33*	dun	38	46.36	122	46.74	1023
s34	cmhz	38	48.65	122	47.43	1029
s35	styz	38	48.71	122	46.92	1052
s36*	gecz	38	48.65	122	48.24	820
s37*	davz	38	45.78	122	48.46	869
s38	dnvs	38	45.75	122	44.34	859
s39	tch	38	47.03	122	44.10	966
s40	sqk	38	49.41	122	48.53	646
s41	pfr	38	44.93	122	44.47	994
s42	ssr	38	44.41	122	42.60	1073
s43	mns	38	46.58	122	42.92	715
s44	wrkz	38	45.77	122	43.36	991
s45	des	38	45.97	122	41.87	552
s46	dvb	38	45.76	122	44.18	832
s47	sb4b	38	48.57	122	49.72	401

Table 2: One-dimensional starting model for the P-wave velocity inversion. The U-N-T model is shown for comparison.

Layer Number	Starting Model (km/s)	U-N-T Starting Model (km/s)	Node depth (ft)	Node depth (km)
2	4.0	4.00	-3000	-0.88
3	4.0	4.00	-1000	-0.29
4	4.4	4.43	1000	0.29
5	5.1	5.12	3000	0.88
6	5.1	5.12	5000	1.47
7	5.4	5.47	7000	2.06
8	5.4	5.47	9000	2.65
9	5.6	5.58	11000	3.23
10	5.6	5.58	13000	3.82
11	5.6	5.58		

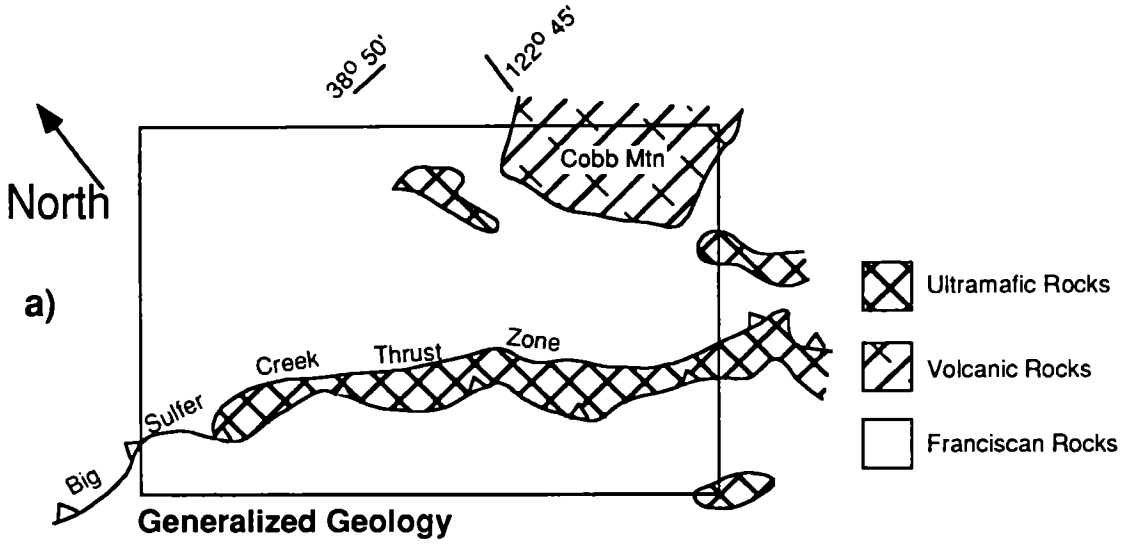

Generalized Geology

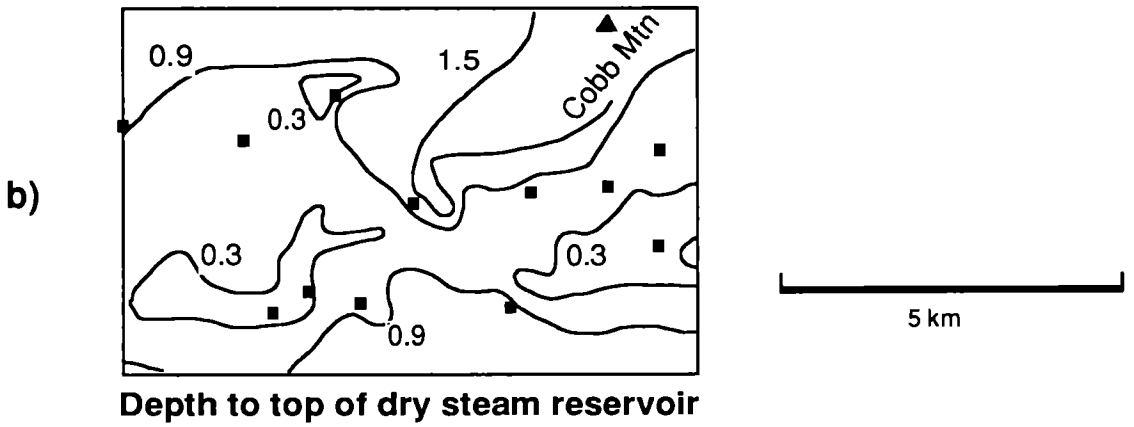

Depth to top of dry steam reservoir

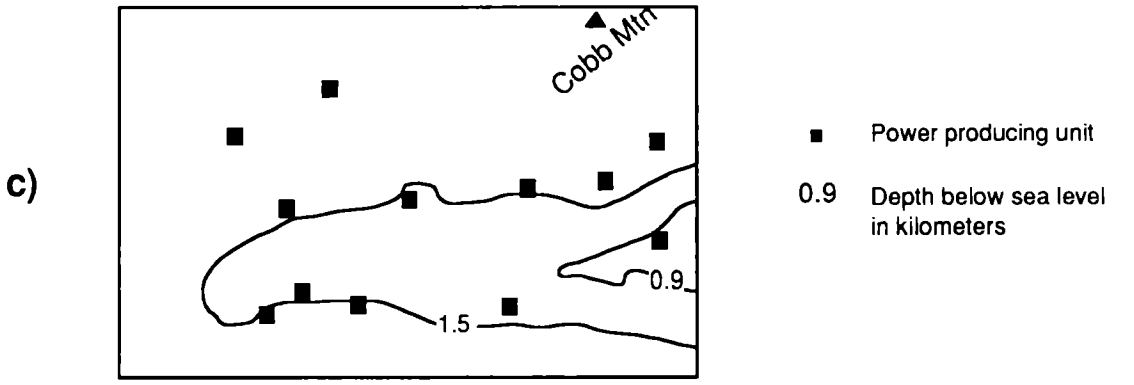

Depth to top of felsite

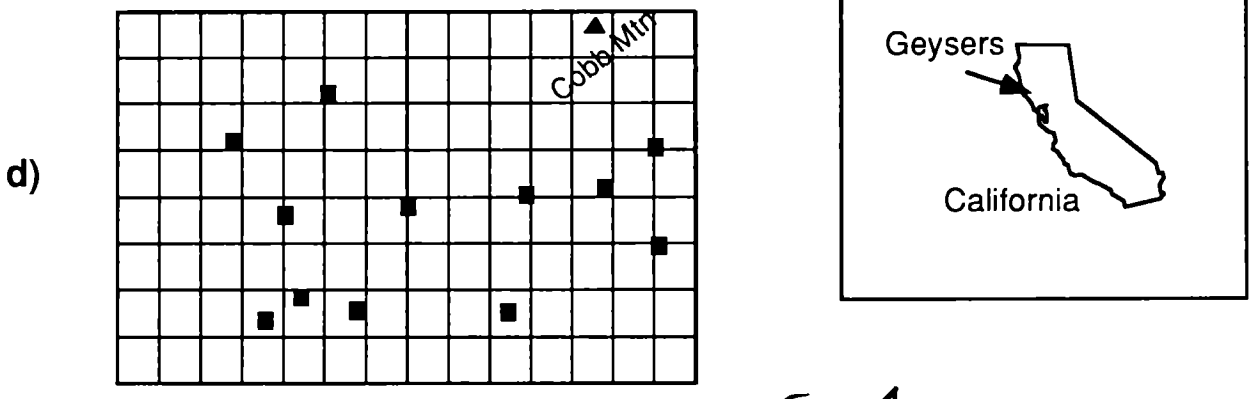

Inversion grid

Fig 1

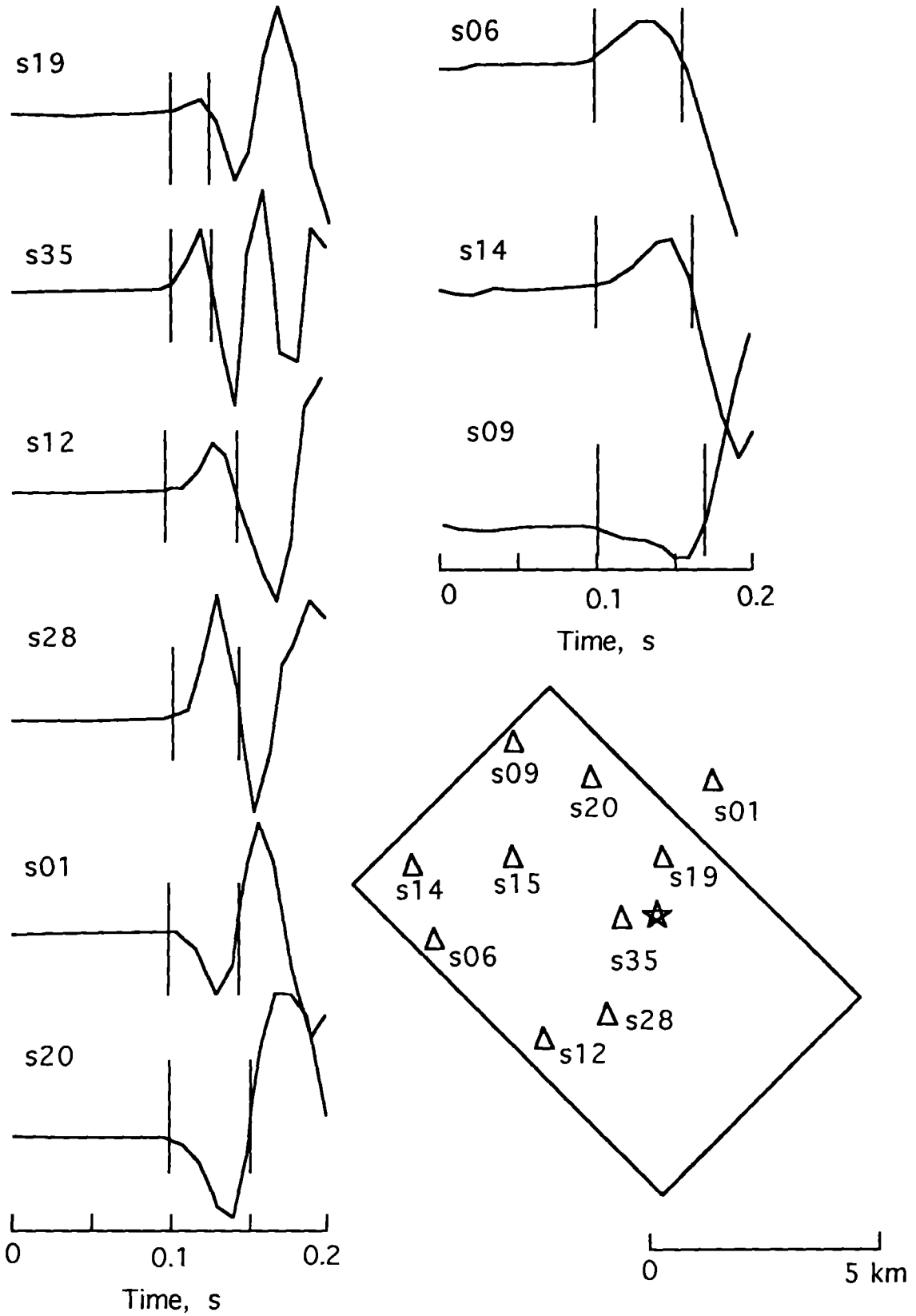
s19
s35
s12
s28
s01
s20
0
0.1
0.2
Time, s
s06
s14
s09
0
0.1
0.2
Time, s
s09
s20
s01
s14
s15
s19
s06
s35
s28
s12
0
5 km

Fig 2

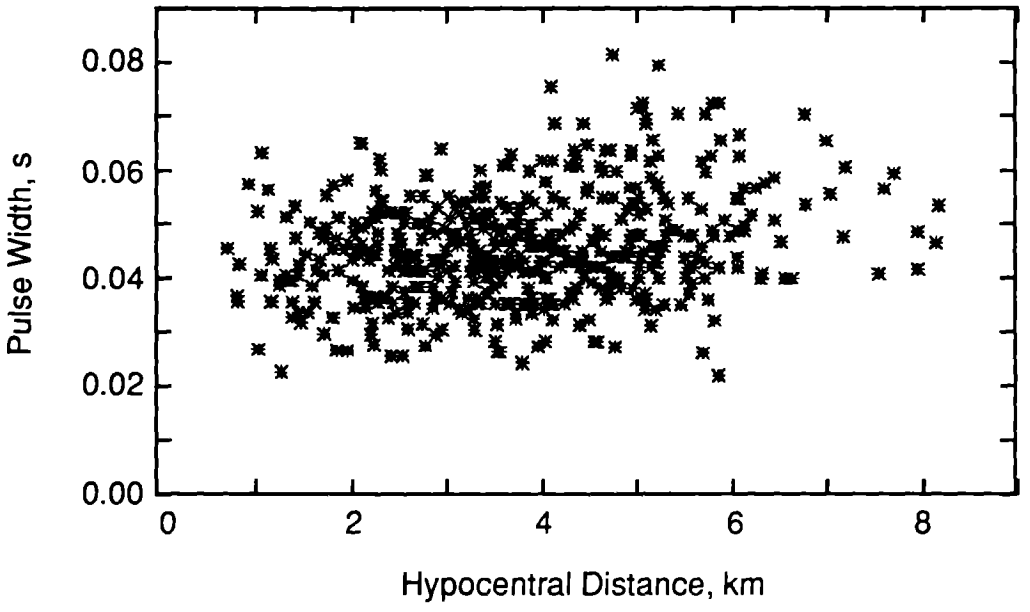
0.08
0.06
0.04
0.02
0.00
Pulse Width, s
0
2
4
6
8
Hypocentral Distance, km

Figure 3

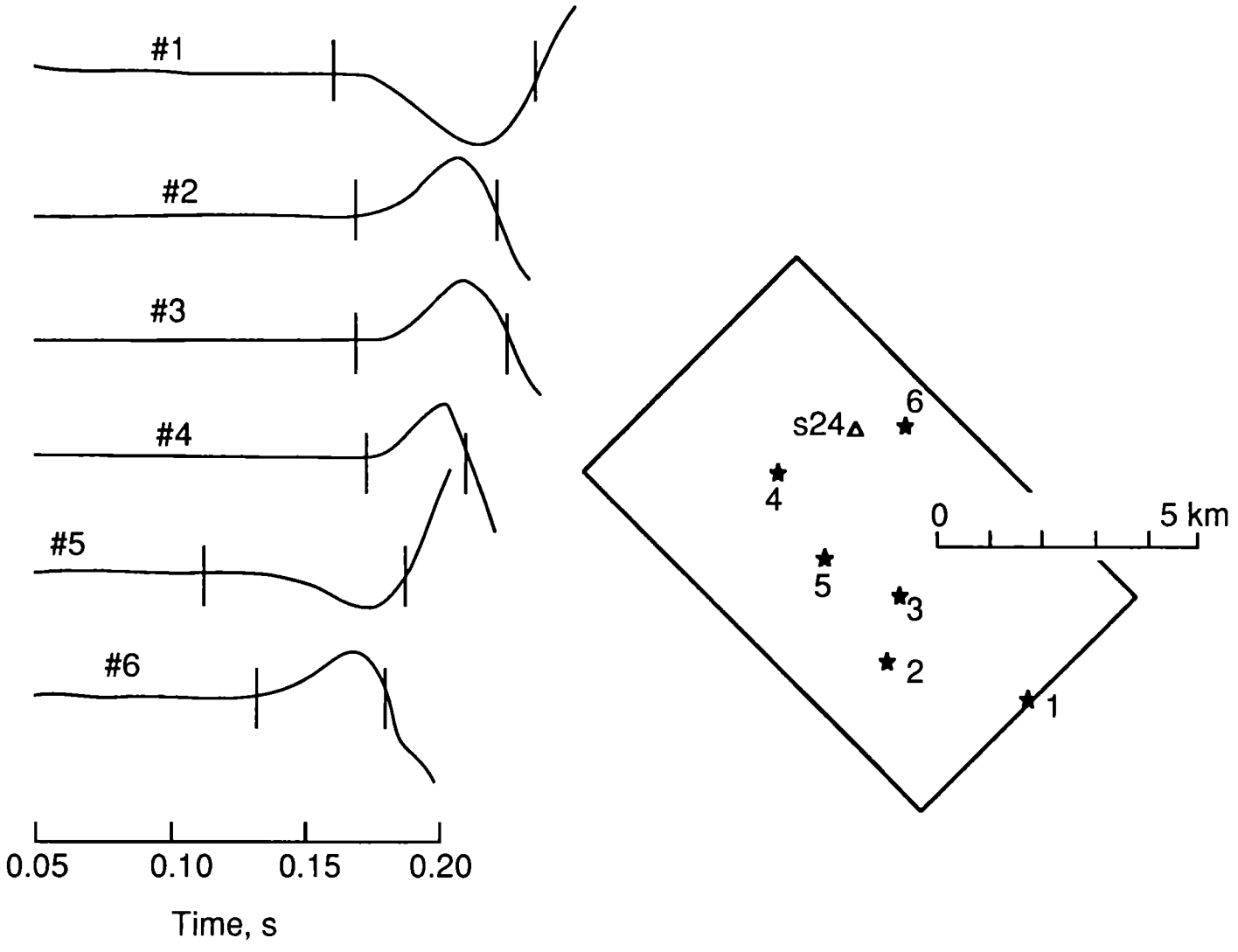

Fig 4

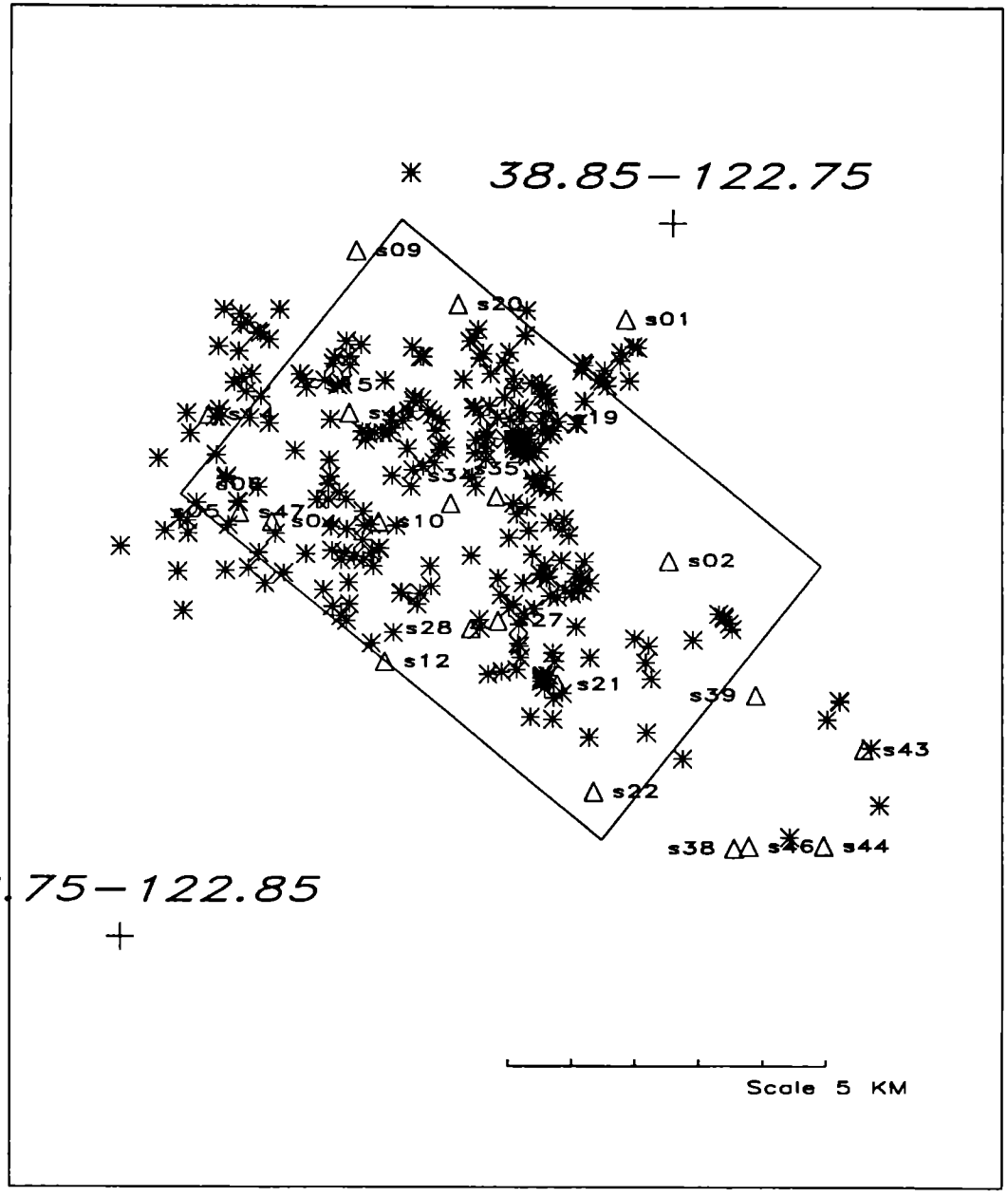

PROJECTION: LAMBERT, CENTER: 38.80 −122.78 0.0
WINDOW CORNERS 38.7150 −122.8700 38.8800 −122.6900

Fig 5

Fig 5

layer01

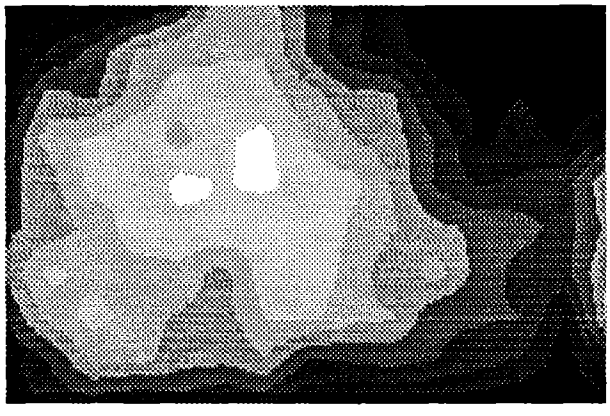

layer02

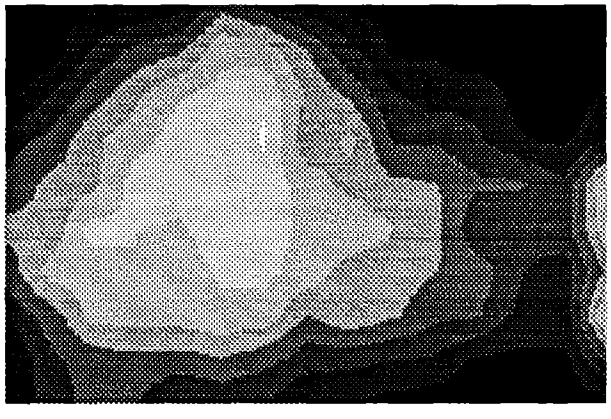

layer03

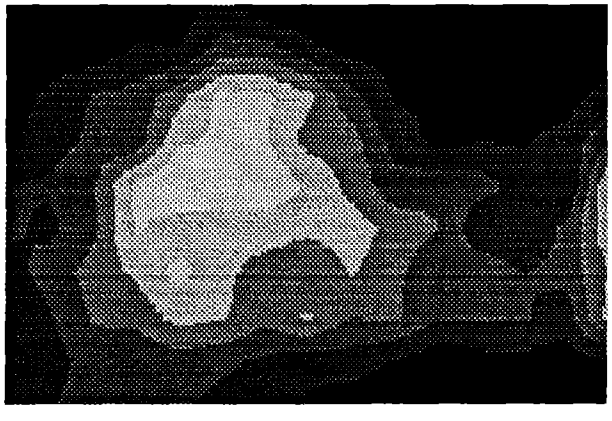

layer04

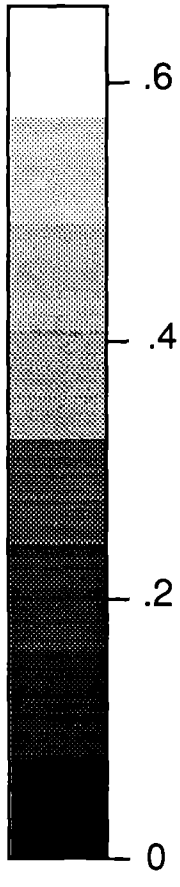

Resolution

Fig 6

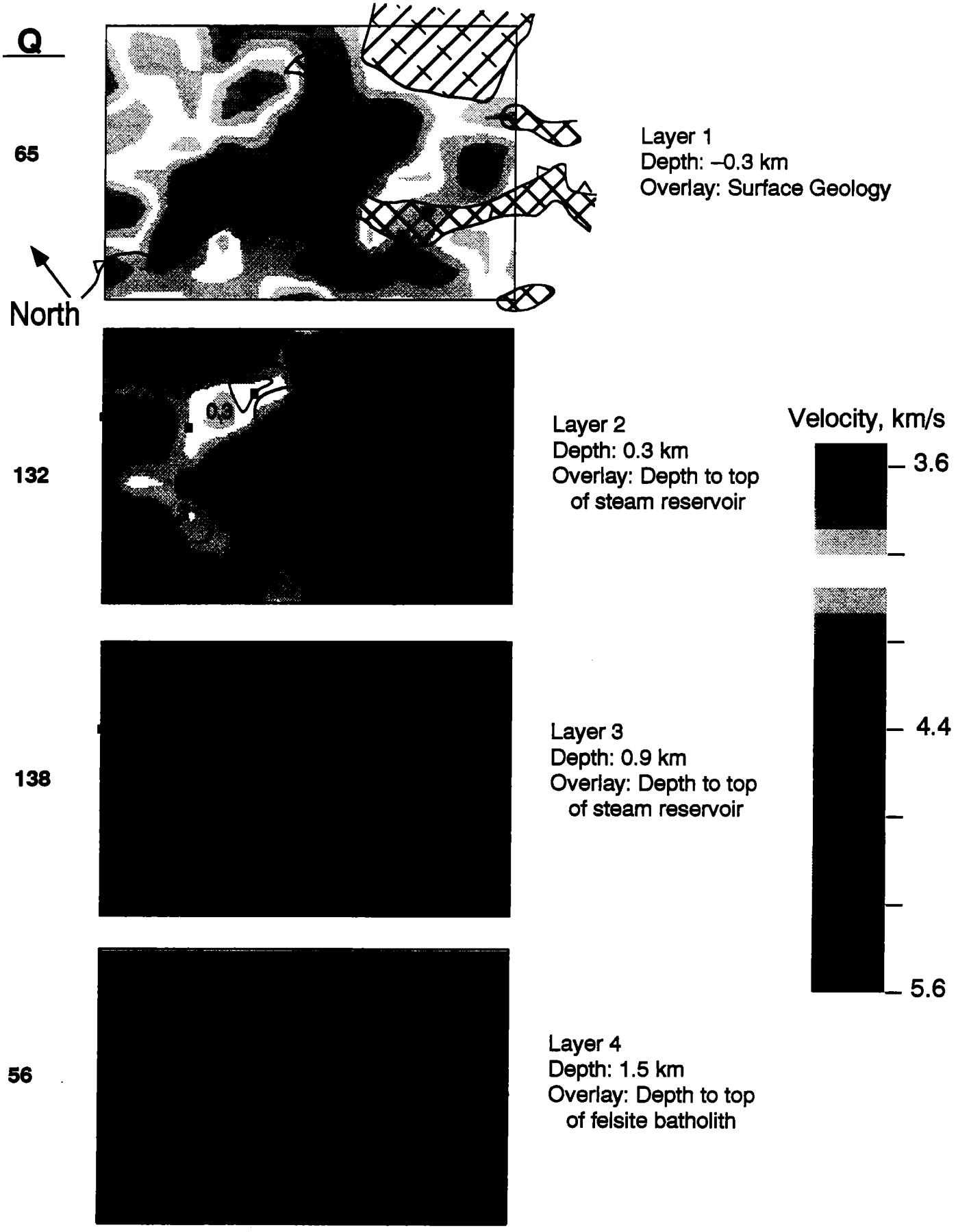
Q
65
North
Layer 1
Depth: –0.3 km
Overlay: Surface Geology
132
Layer 2
Depth: 0.3 km
Overlay: Depth to top
of steam reservoir
Velocity, km/s
3.6
4.4
5.6
138
Layer 3
Depth: 0.9 km
Overlay: Depth to top
of steam reservoir
56
Layer 4
Depth: 1.5 km
Overlay: Depth to top
of felsite batholith

Figure 7